A High-Power Switching Network for a Dual-Mode Antenna

VICTOR J. ALBANESE, SENIOR MEMBER, IEEE, AND DONALD KERBS

Abstract—**A novel hybrid switching network is described in which high levels of RF power (2–3 kW) are controlled and switched over an octave bandwidth in low L band by the use of a relatively low-power level switch matrix used in conjunction with a pair of 8.34-dB (nominal) directional couplers and a phasing network. An alternate design to compactly achieve the same results is also described. The device is for use with a switchable (dual-mode) airborne transmitting antenna. Theoretically predicted performance parameters are graphically presented, along with correlated measured data.**

I. Introduction

A NEED has existed for a circularly polarized airborne antenna, which has the capability of being remotely switched between two modes, here nominally defined as providing "spherical" and "hemispherical" coverage. The antenna mounts on a rotary joint and rotates about a vertical axis within a radome cover of very limited size and contour and is, therefore, severly limited in size and weight. The problem is further compounded by the need for the antenna to transmit several kilowatts of average CW power over an octave frequency range in low L band.

After a number of antenna configurations were considered, a design technique was evolved comprising a pair of special high-power spiral antennas, closely spaced (in wavelengths) back-to-back, and fed by a special purpose switching technique, which provided either full power to one antenna ("single" mode) or half power to each antenna ("dual" mode), while maintaining low voltage standing wave ratio (VSWR) characteristics. The antenna design is in itself unique and may be the subject of a separate paper. It is the intention of this paper, therefore, to describe the high-power switching technique, which was evolved for this application.

The conventional switching methods shown in Fig. 1 were initially considered to produce the "dual" or "single" mode performance and discarded, either because of the adverse effect of changing impedance levels on VSWR or because of the size and weight limitations of the full-power switches.

II. Switching with Tandem 8.34-dB Directional Couplers

The principle of tandem connection of two 8.34-dB (nominal) quarter-wave directional couplers to form a broadband quadrature 3-dB hybrid is well known [1], [2]. The 8.34-dB coupling values produce vector summations

Manuscript received May 5, 1977; revised August 23, 1977.

The authors are with Grumman Aerospace Corporation, Bethpage, NY 11714.

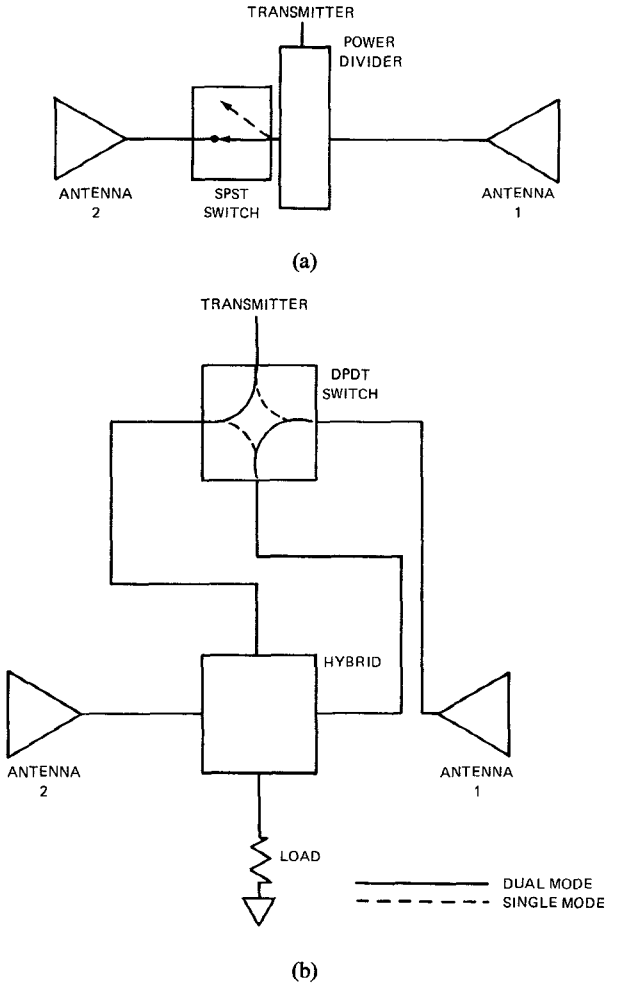

Fig. 1. Conventional switching methods. (a) Power divider with SPST switch. (b) DPDT switch with hybrid.

at the two output ports which result in equal power levels and quadrature phase. This device has a number of advantages over a conventional quarter-wave 3-dB hybrid, most notably in power handling capability, performance insensitivity to tolerance variations, and the elimination of "touchy" tuning devices at the higher frequencies. The use of the tandem couplers in several high-power switching arrangements is described below.

III. Internally Switchable Tandem Coupler

A cross-sectional view of a typical barline directional coupler is shown in Fig. 2. If the coupling value is 3 dB, the ratio of even- to odd-mode impedances [3] is $Z_{0e}/Z_{0o} \approx 5.8$. Assuming $Z_0 = 50\ \Omega$, then $Z_{0e} \approx 120\ \Omega$ and $Z_{0o} \approx 21$

0018-9480/78/0500-0348$00.75

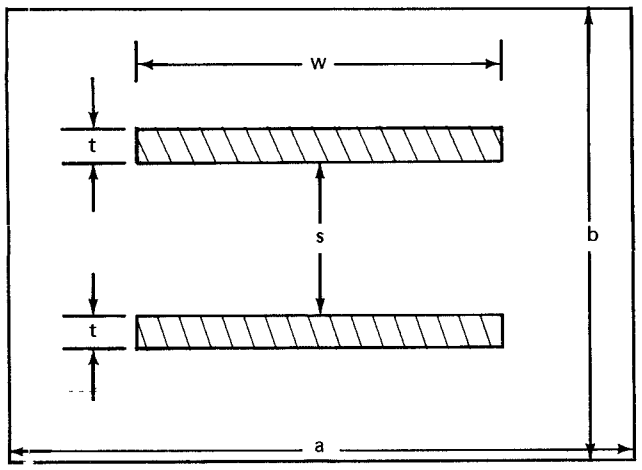

Fig. 2. Barline directional coupler.

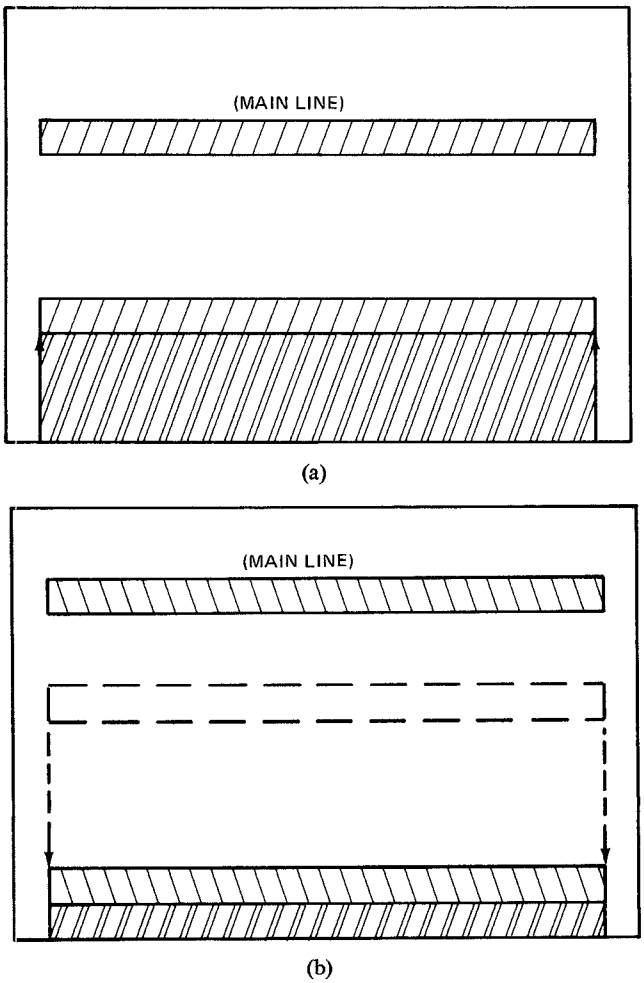

Fig. 3. Directional coupler with movable coupled line. (a) Coupled line shorted to ground. (b) Coupled line withdrawn to ground.

Ω. For an 8.34-dB coupler, $Z_{0e}/Z_{0o} \approx 2.2$, $Z_{0e} \approx 74$ Ω and $Z_{0o} \approx 34$ Ω. The closeness of these impedances to Z_0 suggests that the second or coupled bar could be shorted to ground or withdrawn from proximity to the mainline bar as shown in Figs. 3(a) and 3(b), respectively, with only minimal effect on the mainline impedance and VSWR. If the mainline bar, of a nominally 8.34-dB coupler, is

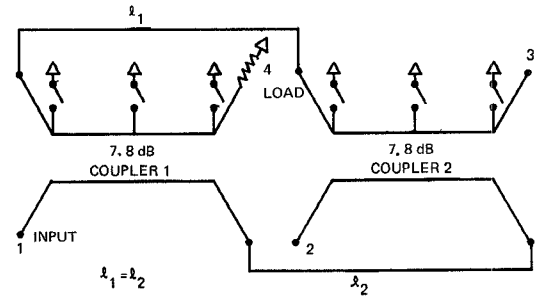

Fig. 4. Schematic of tandem directional couplers. Note: switchable grounds for internally switched device.

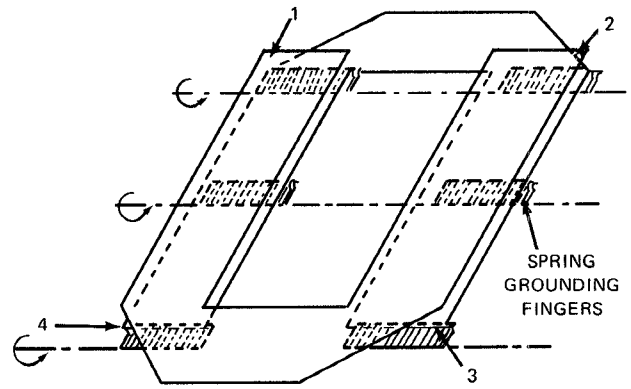

Fig. 5. Switchable tandem directional couplers.

viewed as a modified offset bar, its impedance can be approximated. For several physical configurations corresponding to Figs. 3(a) and 3(b), respectively, the Z_0 of the mainline was calculated as $Z_0(a) = 47$ Ω and $Z_0(b) = 60$ Ω. The theoretical VSWR corresponding to these values was considered acceptable for system operations.

A pair of tandem directional couplers suitable for high-power application and switching is shown schematically in Fig. 4 and in isometric in Fig. 5. Practical design information on barline and stripline couplers may be obtained in the literature [4], [5]. For practical considerations the configuration of Fig. 3(a) is considered superior. To optimize over an approximate octave frequency band, the center frequency coupling value was chosen as 7.8 dB. By experimentation, it was found that three separate shorting plates per coupler (or a total of six for the entire device) situated approximately at each end and the center, and operating with a short rotary motion under each segment of the coupled line was sufficient to provide the desired results. A prototype model of the switching device was fabricated and is shown in Fig. 6. The input connector, port 1, is an EIA 1 5/8″ coaxial fitting and the two output connections, ports 2 and 3, are shown as special barline fittings for convenient mating to the antennas' inputs. Measured data is shown in Fig. 7 for both single- and dual-modes of operation.

It should also be possible, for some applications, to replace the mechanical shorts by solid-state elements situated at approximately the same locations. An analysis of the power which is carried in the coupled line shows that referenced to the input, it varies from 20–30 dB down at port 4 to 7.8 dB opposite port 1 to 3 dB (nominal) at

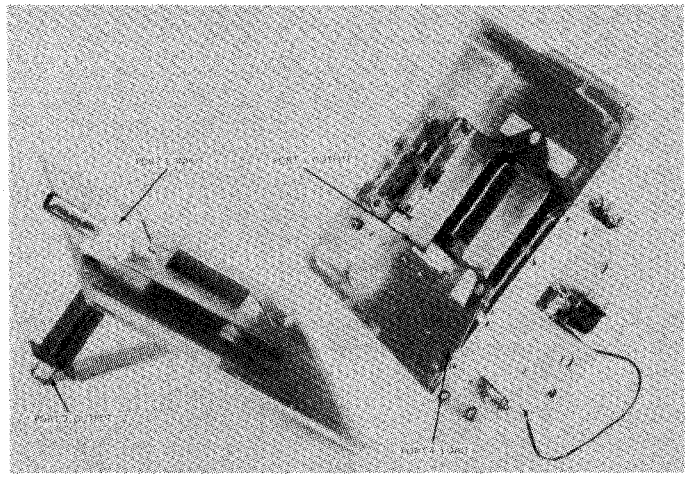

Fig. 6. Prototype internal switching device.

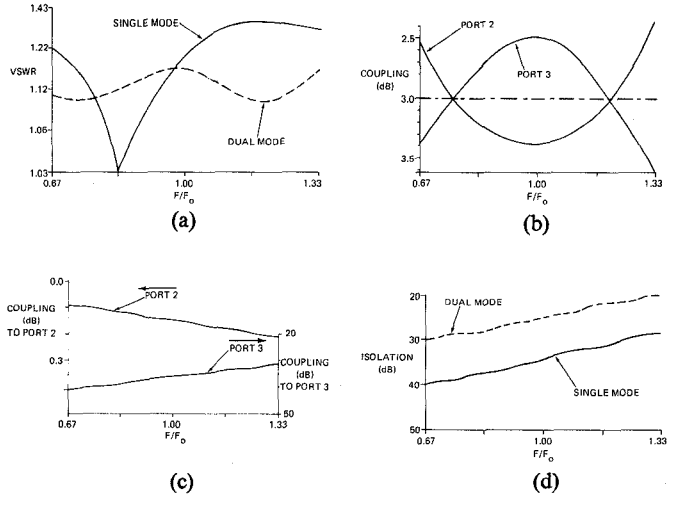

Fig. 7. Measured data, prototype internal switching device. (a) VSWR at port 1. (b) Coupling to ports 2 and 3 for dual mode. (c) Coupling from port 1 to ports 2 and 3 for single mode. (d) Isolation, port 1 to port 4 (matched loads).

port 3. At no point, therefore, does a solid-state element see the full power. A check of the work presently proceeding in the field of high-power switching diodes and phase shifters suggests that this device would be practical in the present L-band application at a power level of several kilowatts CW.

IV. Externally Switchable Tandem Coupler

An alternative exists to the internally switchable device, whereby high levels of RF power can be controlled and switched with the use of a matrix of standardized relatively low-power level switches and phase shifters appropriately connected to the couplers. Referring to Fig. 8, it is seen that with the switches in the positions to provide phase shift φ_1, the total insertion phases of the two interconnecting lines (paths A and B) are identically equal and the power splits equally between ports 2 and 3 with quadrature phase (vectorially shown in Fig. 9(a)). It can also be shown that if, with the switches in the positions to provide phase shift φ_2, the total insertion phase of paths A and B differ by $\pm 180°$ so that $\varphi_A = \varphi_B \pm 180°$, all the input power will arrive at port 2 and no power will be

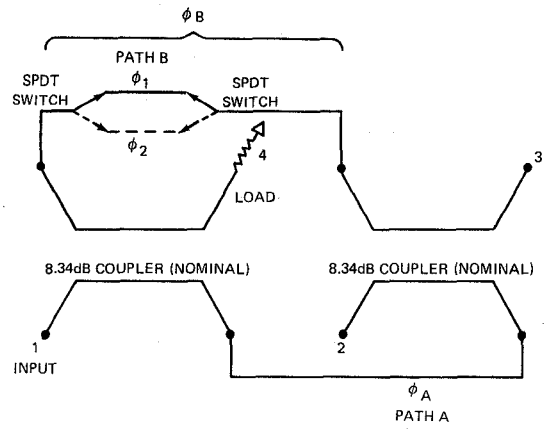

Fig. 8. Schematic of externally switchable couplers.

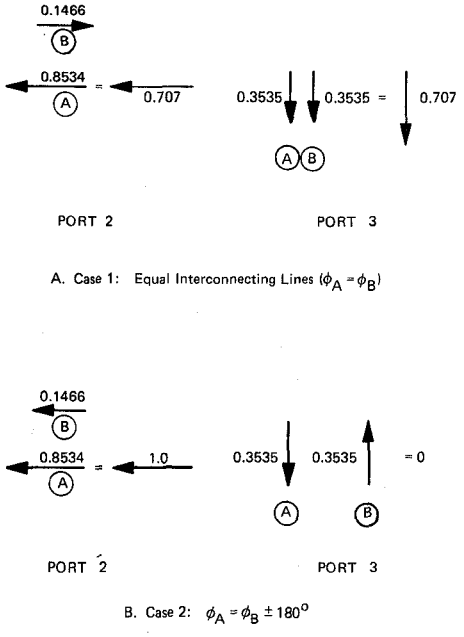

Fig. 9. Voltage vector relationships at ports 2 and 3 with input at port 1 (F_0).

present at port 3. This can be simply shown for the exact vector relationship of the 8.34-dB couplers at F_0 by referring to Fig. 9(b).

The equations governing the distribution of power to ports 2 and 3 for varying values of coupling and frequency are derived below for both modes of operation.

For a single coupler with input to port 1, coupled output at port 2′, and main output at port 3′

$$\frac{E_2'}{E_1} = K_{12}' = \frac{jc \sin\theta}{\sqrt{1-c^2}\cos\theta + j\sin\theta}$$

and

$$\frac{E_3'}{E_1} = K_{13}' = \frac{\sqrt{1-c^2}}{\sqrt{1-c^2}\cos\theta + j\sin\theta}$$

where c is the coupling factor or midband value of coupling, θ is the electrical length of the coupled line and is equal to $\pi/2$ at midband frequency, F_0, and the output ports for the single coupler have been primed to differen-

tiate from the ports of the combined tandem coupler. The above equations may be rewritten in the following form:

$$|K'_{12}| = \frac{c \sin\theta}{\sqrt{1-c^2\cos^2\theta}}$$

$$\theta'_{12} = \frac{\pi}{2} - \tan^{-1}\left(\frac{\tan\theta}{\sqrt{1-c^2}}\right)$$

$$|K'_{13}| = \frac{\sqrt{1-c^2}}{\sqrt{1-c^2\cos^2\theta}}$$

$$\theta'_{13} = -\tan^{-1}\left(\frac{\tan\theta}{\sqrt{1-c^2}}\right)$$

$$\theta'_{12} = \frac{\pi}{2} + \theta'_{13}.$$

For a pair of identical and synchronously tuned tandem couplers, with interconnecting lines φ_A and φ_B as shown schematically in Fig. 8, where

$$\varphi_A = \varphi_B + \beta$$

$$\frac{E_2}{E_1} = \left[|K'_{13}|^2 \angle 2\theta'_{13}\right] + \left[|K'_{12}|^2 \angle \pi + 2\theta'_{13} + \beta\right]$$

and

$$\frac{E_3}{E_1} = \left[|K'_{12}||K'_{13}| \angle 2\theta'_{13} + \frac{\pi}{2}\right] + \left[|K'_{12}||K'_{13}| \angle 2\theta'_{13} + \frac{\pi}{2} + \beta\right].$$

A. Dual Mode

When $\beta = 0$ an inspection of the above equations shows that the magnitudes of the vector sums are

$$\left|\frac{E_2}{E_1}\right| = |K'_{13}|^2 - |K'_{12}|^2 = \frac{1-c^2(1+\sin^2\theta)}{1-c^2\cos^2\theta}$$

and

$$\left|\frac{E_3}{E_1}\right| = 2|K'_{12}||K'_{13}| = \frac{2c\sqrt{1-c^2}\,\sin\theta}{1-c^2\cos^2\theta}.$$

B. Single Mode

When $\beta = \pi$, the equations reduce to

$$\left|\frac{E_2}{E_1}\right| = |K'_{13}|^2 + |K'_{12}|^2 = \frac{1-c^2+c^2\sin^2\theta}{1-c^2\cos^2\theta} = \frac{1-c^2(1-\sin^2\theta)}{1-c^2\cos^2\theta} = 1$$

and

$$\left|\frac{E_3}{E_1}\right| = |K'_{12}||K'_{13}| - |K'_{12}||K'_{13}| = 0.$$

Note that the relationships for the case of $\beta = \pi$ are independent of frequency if β is independent of frequency. For the specific case where β is frequency dependent, as in the use of a coaxial cable which is $\lambda/2$ at F_0, the above two equations may be reduced to

$$P_{12} = \left(\frac{E_2}{E_1}\right)^2 = \frac{(1-c^2)^2 + c^4\sin^4\theta + 2(1-c^2)c^2\sin^2\theta\cos\gamma}{(1-c^2\cos^2\theta)^2}$$

$$P_{13} = \left(\frac{E_3}{E_1}\right)^2 = 2\left(\frac{c\sqrt{1-c^2}\,\sin\theta}{1-c^2\cos^2\theta}\right)^2(1-\cos\gamma)$$

where $\beta = \pi F/F_0$ and $\gamma = \pi - \beta = \pi(1-(F/F_0))$.

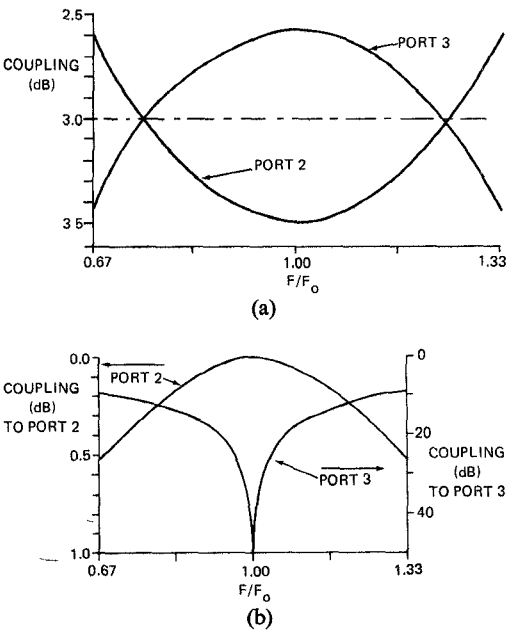

Fig. 10. Calculated performance of dual-mode switching network. (a) Coupling from port 1 to ports 2 and 3 for dual mode ($\phi_A = \phi_B$). (b) Coupling from port 1 to ports 2 and 3 for single mode ($\phi_A = \phi_B \pm 180°$ F/F_0, phase shift achieved with cable).

These equations were programmed onto the IBM 360 and performance was calculated over an approximate octave frequency band. Two conditions of phase shift were considered for the case of single output only to port 2; namely that the 180° differential phase shift is either frequency invariant as approximated by a Schiffman phase shifter [6] network or that it varies linearly with frequency as with a coaxial cable. The calculated lossless performance of the full network for both modes of operation with frequency varying phase shift ($\beta = \pi F/F_0$) is shown in Fig. 10. Also optimized center frequency coupling to achieve minimum deviation from equal power split in the dual mode was found to be approximately 7.83 dB.

V. Schiffman Phase Shifter

Since a 180° differential phase shift is required between paths A and B, but a conventional Schiffman type phase shifter produces a 90° differential phase shift, a "double" network is required. The required condition is shown in Fig. 11. For the dual mode, $\varphi_A = \varphi_{B1}$, and this is achieved as before by simply balancing overall line lengths. For the single mode, path A has a line length, which is 540° longer than the line length (including switches) of path $B2$. The $B2$ path is completed with the inclusion of the dual Schiffman sections.

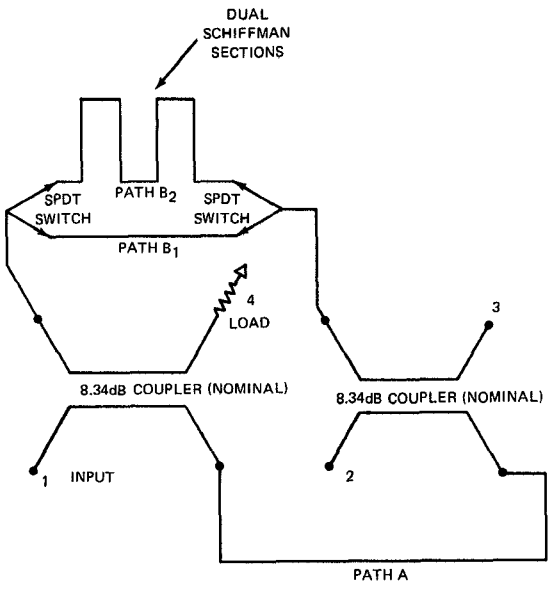

Fig. 11. Switchable frequency invariant (nominal) 180° phase shift network with tandem couplers.

VI. Practical Implementation

A. Switch Matrix

An inspection of Fig. 8 will reveal that the power traveling along path B is diminished from the transmitter input by the coupling factor of the first directional coupler. For the practical broadband case under consideration, the power, therefore, at F_0 would be 7.8 dB down from several kilowatts (average). At other frequencies, path B power would be even lower. It was possible, therefore, to use standard, commercially available, intermediate power, latching switches with TNC connector inputs for this application. These switches are presently in wide use for a variety of applications; they are relatively inexpensive and highly reliable.

A transfer switch (DPDT) was also considered for use, but the SPDT pair were found to better fit physically into the application. Although the advantages of the Schiffman network over the frequency sensitive coaxial line phase shifter are obvious, packaging space was so limited in the switchable antenna assembly that the latter was chosen for use.

B. Tandem Directional Couplers

The first brassboard coupler assembly was designed to mate with EIA, 1 5/8″ coaxial input line and was designed with air dielectric, except for transitions and support leads. Because of the high-power requirement and the need to operate at high altitude (40 000 ft) and to minimize insertion loss in the brass model, the dimensions were somewhat oversized with the bar width W and the outer ground plane spacing b as shown in Fig. 4, both 1.5″. The remaining dimensions a, t, and s were, respectively, chosen as 3.0″, 0.063″, and 0.5.″ Output ports 2 and 3 were terminated in barline, which mated with corresponding barline on the antenna feeds. Path A was completed with a prescribed length of high-power cable, formed to fit within the overall brassboard packaging constraints.

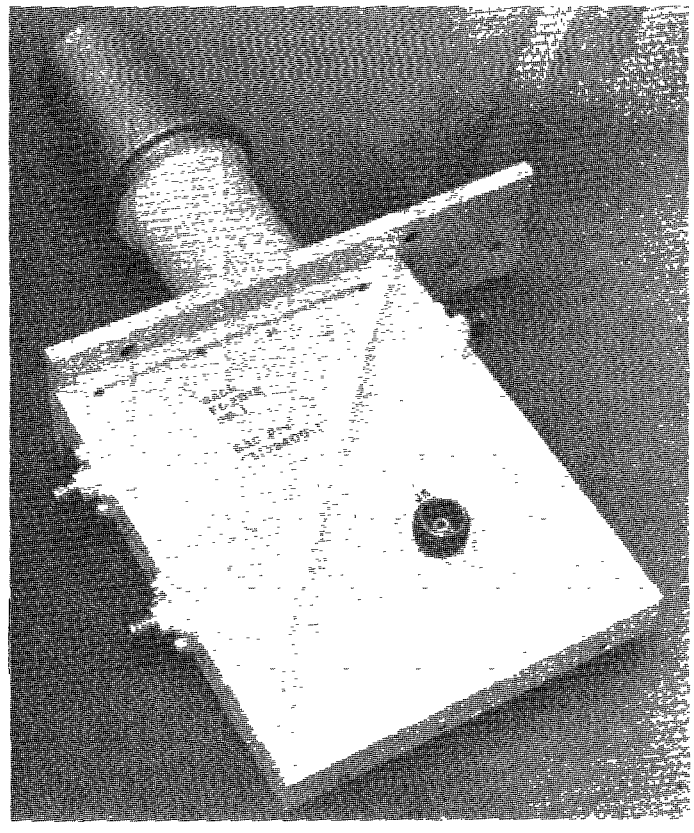

Fig. 12. Prototype dual coupler.

A prototype tandem coupler, shown in Fig. 12, was developed under subcontract. It was designed completely within a teflon dielectric and incorporated path A as an enclosed meander line. Ports 2 and 3 terminated in a more practical modified height SC connector.

C. Dummy Load

Although the isolation to port 4 with ports 2 and 3 terminated in matched loads exceeded 20 dB in the brassboard, it should be obvious that the quadrature phase relationships at the output ports, when the network is operating in the dual mode, will result in the reflected power (VSWR) from the antennas largely summing in port 4. In fact this does occur and the port 1 to port 4 isolation degrades to approximately 10 dB (for the worst case phasing of 1.65 VSWR's terminating ports 2 and 3). The dummy load, therefore, must be capable of handling several hundred watts of average power without overheating. Size and weight were also of prime importance. A special finned load was developed under subcontract. It weighed less than 2 lb and was mechanically designed to mount against the metal cavity bodies of the antennas for additional heat sinking.

With regard to disposal of the power at port 4, an obvious question would be, "Why not terminate port 4 in a judiciously located short circuit so that the power could be rereflected to the antennas and thereby reradiated?"

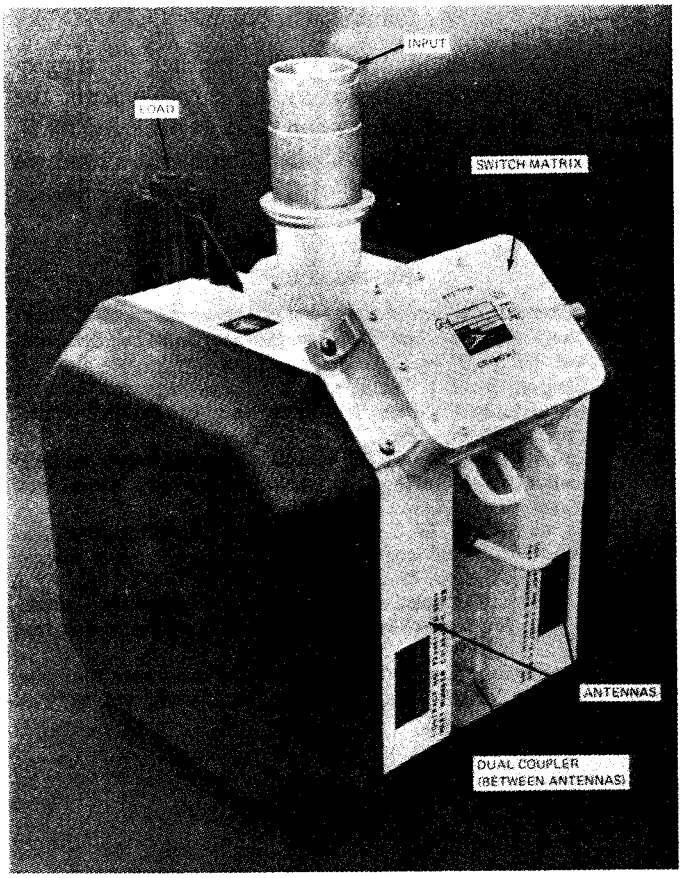

Fig. 13. Prototype antenna assembly.

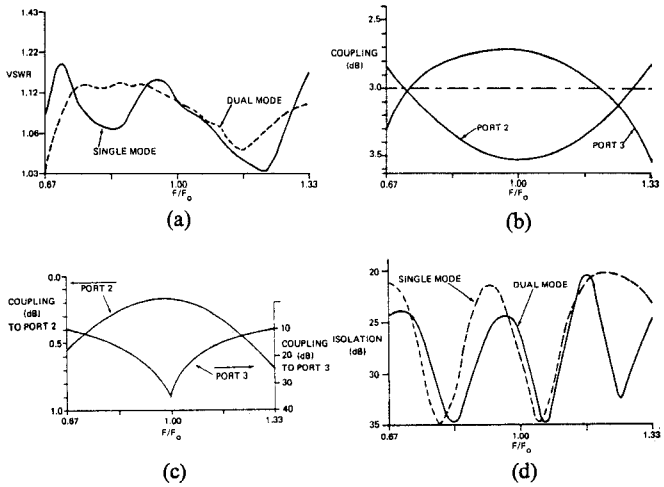

Fig. 14. Measured data, prototype external switch matrix/coupler subassembly. (a) VSWR at port 1. (b) Coupling to ports 2 and 3 for dual mode. (c) Coupling from port 1 to port 2 and 3 for single mode. (d) Isolation, port 1 to port 4 (matched loads).

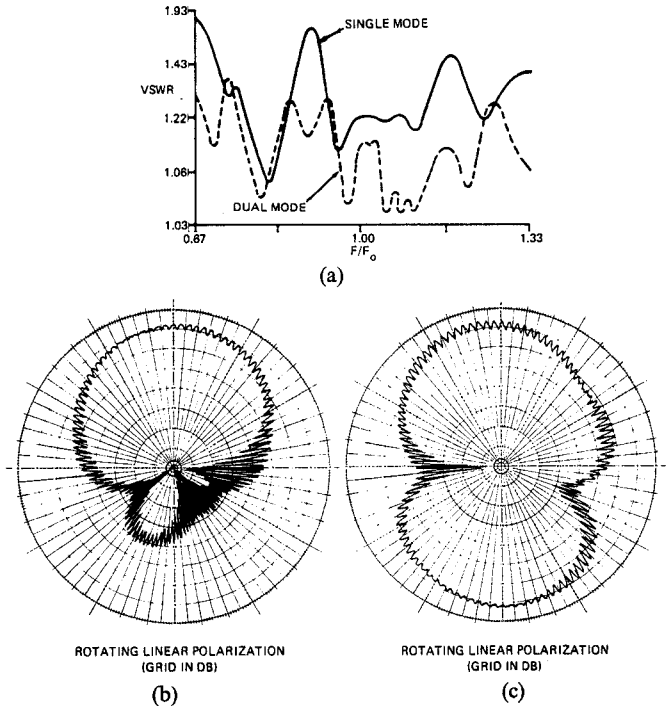

Fig. 15. Measured data, full prototype antenna assembly. (a) Input VSWR. (b) Single-mode radiation pattern at F_0. (c) Dual-mode radiation pattern at F_0.

The answer lies in the rather electrically long insertion phases of paths A and B, which on an absolute basis are varying rapidly with frequency, so that the phases of the rereflected voltage vectors arriving at ports 2 and 3 are rather arbitrary. The net result is that the balance of power radiated would be appreciably disturbed.

D. Full Antenna Assembly

The complete prototype antenna assembly is shown in Fig. 13. The cavity-backed spiral antennas are mounted within the dark-colored radomes. The input coaxial line is one-half of the rotary joint from which the entire assembly is suspended. The switching control voltage is routed to the switch matrix through a special slip ring assembly, which was developed for this purpose.

VII. Measured Data

Complete measured data was taken on each of the prototype components, on the switch matrix/tandem coupler subassembly and on the full switchable antenna assembly. The latter two are shown in Figs. 14 and 15 and include the internal dissipative losses.

A comparison of the performance of the internal and external switching devices can be made by reviewing Figs. 7 and 14. Note that in general the insertion losses are somewhat lower for the internal device, which has larger air-filled lines and does not suffer from the "indirect" loss of the switch matrix. Single-mode coupling for the external device follows the predicted form and port 4 isolation is cyclical, as might be expected for an imperfectly matched hybrid with relatively long interconnecting cables. For the internal switching device the excellent single-mode isolation reflects the effectiveness of the electrical shorting mechanism and the port 4 isolation is closer to that expected for a well-designed coupler.

It should also be noted that the pattern shown in Fig. 15 is near optimum in the single mode since it was taken at midband frequency. The back lobe will increase at band edges in accordance with the higher power reaching port 3 of the coupler. Lobe unbalance is near maximum in

the dual-mode pattern at midband and would also occur at the band edges (see Fig. 14a).

Both breadboard and prototype equipments were subjected to high power, at sea level and at a simulated altitude of 40 000 ft with no apparent damage or degradation in performance.

It is planned in the future to extend this design into the next higher frequency band with a high to low frequency ratio of 2.5 and also at a power level of several kilowatts CW average.

VIII. Conclusions

A class of switches in several different versions has been designed, which enables the control of high levels of RF power with only intermediate power rated switching elements. Solid-state versions could also be evolved. The power division between the two output ports can be made nominally equal, or all the power can be made to appear at a single port. If a variable phase shifter were used in the switch matrix, other power divisions between these two extremes would be possible. Extremely broad bandwidth requirements could be accommodated with multisection couplers.

Acknowledgment

The authors wish to acknowledge the helpful suggestions of J. Goff, who designed the antenna elements, the mechanical design and integration support provided by B. Behrenfeld and T. Kober, and the computerized analysis provided by H. Stadmore, all of the Grumman Aerospace Corporation.

References

[1] G. D. Monteath, "Coupled transmission lines as symmetrical directional couplers," *Proc. Inst. Elec. Eng. (London) Radio and Electronic Eng.*, vol. 102, pt. B, pp. 383–392, May 1955.

[2] J. P. Shelton, Jr., J. J. Wolfe, and R. C. VanWagoner, "Tandem couplers and phase shifters for multi-octave bandwidth," *Microwaves*, pp. 14–19, Apr. 1965.

[3] S. B. Cohn, "Characteristic impedances of broadside-coupled strip transmission lines," *IRE Trans. Microwave Theory Tech.*, vol. MTT-8, pp. 633–637, Nov. 1960.

[4] J. K. Shimizu and E. M. T. Jones, "Coupled-strip-transmission line filters and directional couplers," *IRE Trans., Microwave Theory Tech.*, vol. MTT-4, pp. 75–81, Apr. 1956.

[5] W. J. Getsinger, "Coupled rectangular bars between parallel plates, "*IRE Trans., Microwave Theory Tech.*, vol. MTT-10, pp. 65–72, Jan. 1962.

[6] B. M. Schiffman, "A new class of broad-band microwave 90-degree phase shifters," *IRE Trans. Microwave Theory Tech.*, vol. MTT-6, pp. 232–237, Apr. 1958.

Characteristics of High-Power Breakdown at 28 GHz

MAKOTO NAKAMURA, TAKAYA SAITO, AND MINORU KURAMOTO

Abstract—**Characteristics of arcs resulting from high-power breakdown in a waveguide at 28 GHz were determined as a function of CW power level. The radio frequency power reflected from and absorbed in arcs as well as the arc velocity were measured. In addition, the spectrum of the arc light and the track on the surface in a waveguide caused by an arc were evaluated. Comparing the velocity of an arc at 28 GHz with that at about 10 GHz, it was found that the velocity of the arc is proportional to the square of the electric field strength but depends very little on radio frequency.**

I. Introduction

AN ARC resulting from electric breakdown in a high-power satellite communication transmitter travels toward the power source and can damage the window of the high-power electron tube. It is therefore important in the design of high-power transmitters to evaluate the characteristics of arcs.

Manuscript received March 2, 1977; revised August 23, 1977.

The authors are with Yokosuka Electrical Communication Laboratory, N.T.T., Take, Yokosuka-shi, Kanagawa-ken, 238-03, Japan.

In this paper, the characteristics of arcing in WRI-260 waveguide (8.6 mm×4.3 mm) at 27.95 GHz is described. The velocity of an arc and the power reflected from and absorbed by an arc were measured in a series of experiments. In addition, the spectrum of the arc light and the track on the surface in a waveguide caused by an arc were evaluated. Finally, the measured velocity of arcs was compared with that of arcs at about 10 GHz reported by May [2] to determine the effect of the radio frequency dependence.

II. Test Setup

The test setup used for the experiments reported here is illustrated in Fig. 1. The incident radio frequency (RF) power is supplied from an air cooled traveling-wave tube (TWT) high-power transmitter to the test circuit using WRI-260 rectangular waveguide, and is controlled by a ferrite variable attenuator placed at the output of the transmitter.

0018-9480/78/0500-0354$00.75